INTERNATIONAL JOURNAL FOR NUMERICAL METHODS IN FLUIDS, VOL. 14, 1019–1036 (1992)

FINITE ELEMENT MODELLING OF NATURAL-CONVECTION-CONTROLLED CHANGE OF PHASE

A. S. USMANI, R. W. LEWIS AND K. N. SEETHARAMU*

Institute for Numerical methods in Engineering, University College of Swansea, Swansea, U.K.

SUMMARY

The problem of phase change in the presence of natural convection has been investigated. A model has been proposed based on the treatment of the release/absorption of latent heat as a heat source/sink in combination with the standard Galerkin finite element method with a primitive variable formulation on a fixed grid. To demonstrate the capabilities of the model, three cases of phase change of an aluminium alloy in the presence of natural convection are considered, i.e. solidification, melting and combined solidification and melting. The solidification of water in a square cavity is modelled as another example, taking into account the density extremum, and the results are compared with a previously published work.

KEY WORDS Natural convection Phase change Heat source method Solidification Melting Square cavity Water

1. INTRODUCTION

Many aspects of materials-processing methods, including purification of metals, growth of pure crystals from melts and solutions, solidification of castings, and ingots, welding, electro slag melting, zone melting, thermal energy storage using phase change materials, etc., involve melting and solidification. In all cases these phase transformation processes are accompanied by either absorption or release of thermal energy. A moving boundary exists that separates the two phases of differing thermophysical properties and at which thermal energy is absorbed or liberated. The heat transfer processes occurring are complex, the cooling rates employed range from 10^{-5} to 10^{10} K s^{-1} and corresponding solidification systems extend from several metres to a few micrometres. These various cooling rates produce different microstructures and consequently a variety of thermomechanical properties.

Numerical methods have long been employed to predict the phase change behaviour of such systems to enable better control over them. The early attempts were based upon the analysis of conduction heat transfer[1,2] only, since this is sufficient for many cases; however, many analyses have appeared in the past decade taking into account natural convection effects. Convection cannot be neglected in many cases of practical interest.[3–5] In a finite element method context a significant contribution was made by Gartling,[6] who made use of the Boussinesq approximation and the enthalpy method in solving the Navier–Stokes and energy equations. Later, Morgan[7] presented an explicit finite element algorithm for the solution of the basic equations

* Visitor from Indian Institute of Technology, Madras, India.

0271-2091/92/091019–18$09.00

Received November 1990
Revised August 1991

describing combined conductive and convective transfer of heat in a material undergoing a liquid/solid change of phase in a cylindrical thermal cavity.

The enthalpy method suffers from a number of deficiencies as discussed in References 8 and 9. In this paper we have used a method[10] which treats the release/absorption of latent heat as a fictitious heat source/sink in combination with the standard Galerkin finite element method based on a mixed formulation with the primitive variables[11] using a fixed mesh. Some examples of phase change in the presence of natural convection are presented after a brief review of the numerical method.

2. GOVERNING DIFFERENTIAL EQUATIONS

The basic principles of conservation may be invoked to obtain the equations that govern the transfer processes accompanying phase change, namely the conservation of mass, momentum and energy. All these quantities that must be conserved can be transported within the domain of interest by two modes, i.e. diffusion and convection.

Conservation of mass

$$\nabla \cdot \mathbf{v} = 0, \tag{1}$$

where $\mathbf{v}$ represents the velocity.

Conservation of momentum

$$\rho \frac{\mathrm{D}\mathbf{v}}{\mathrm{D}t} = \nabla \cdot \boldsymbol{\tau} + \rho \mathbf{g}, \tag{2}$$

where $\boldsymbol{\tau}$ is the stress tensor, ρ and $\mathbf{g}$ are the density and gravitational acceleration respectively and $\mathrm{D}/\mathrm{D}t$ represents the total or substantial derivative.

Conservation of energy

$$\rho c \frac{\mathrm{D}T}{\mathrm{D}t} = \nabla \cdot k \nabla T + \dot{Q}, \tag{3}$$

where c and k are the specific heat and thermal conductivity respectively, T is the temperature and $\dot{Q}$ is the rate of internal heat generation.

In natural convection problems the effect of temperature on flow can be included in the equations by involving the Boussinesq approximation, in which case equation (2) is written as

$$\rho \frac{\mathrm{D}\mathbf{v}}{\mathrm{D}t} = \nabla \cdot \boldsymbol{\tau} + \rho \mathbf{g} \beta (T - T_{\mathrm{r}}), \tag{4}$$

where β is the coefficient of thermal expansion and T_{r} is a reference temperature.

3. BOUNDARY CONDITIONS

The Dirichlet or essential boundary conditions as applicable to the Navier–Stokes equations and energy equations are the specified velocities or temperature at the boundaries. The pressure may not be specified at the boundaries since it is an implicit variable in an incompressible flow[12] which

'adjusts' itself to deliver a solenoidal velocity field. However, in the case of contained flow, i.e. specified velocities on all boundaries, it must be specified at least at one point as a datum.

The Neumann or natural boundary conditions for the Navier–Stokes equations can be the normal and tangential traction forces specified as

$$f_n = -P + 2\mu \frac{\partial u_n}{\partial n}, \tag{5}$$

$$f_\tau = \mu \left(\frac{\partial u_n}{\partial \tau} + \frac{\partial u_\tau}{\partial n} \right), \tag{6}$$

where n and τ are the unit normal and tangent vectors respectively, P is the pressure and μ is the dynamic viscosity. For the energy equation the general Neumann boundary condition is

$$k \frac{\partial T}{\partial n} + q + h(T - T_a) = 0, \tag{7}$$

where q, h and T_a are the specified boundary heat flux, the convective heat transfer coefficient and the ambient temperature respectively.

4. FINITE ELEMENT FORMULATION

The conservation equations and the boundary conditions may be discretized spatially to obtain the finite element equations. The conventional Galerkin weighted residual technique is the usual way of achieving such a discretization, which will only briefly be presented in this paper. More detailed theoretical treatment can be found in standard texts such as References 13 and 14.

4.1. Spatial discretization

The field variables involved in the governing equations, i.e. temperature (T), velocities ($\mathbf{v}$) and pressure (P), are approximated over each element in terms of the nodal values by shape functions which are written as

$$\mathbf{v}_e = \sum_{i=1}^{n} N_i v_i, \qquad T_e = \sum_{i=1}^{n} N_i T_i, \qquad P_e = \sum_{i=1}^{n'} N_i' P_i, \tag{8}$$

where n represents the number of velocity and temperature nodes in element e and n' the pressure nodes. Similarly, N represents quadratic shape functions for velocity and temperature interpolation and N' represents linear shape functions for pressure interpolation. This is termed the mixed formulation. As defined in Reference 15, mixed formulations are those which result from approximating differential equations in which the variables can be reduced by elimination. Often such formulations are equivalent to applying Lagrangian constraints and result in equations of the form

$$\begin{bmatrix} A & B \\ B^{\mathrm{T}} & 0 \end{bmatrix} \begin{pmatrix} x \\ y \end{pmatrix} = \begin{pmatrix} f_1 \\ f_2 \end{pmatrix},$$

where x are the primary variables and y are the constraint variables. This, in spite of the definition, results in an increase in the number of variables, i.e. the extra constraint variables. This form is widely used for the incompressible flow equations and results in matrices of the form

$$\begin{bmatrix} K & C \\ C^{\mathrm{T}} & 0 \end{bmatrix} \begin{pmatrix} u \\ P \end{pmatrix} = \begin{pmatrix} f \\ 0 \end{pmatrix},$$

where u and P are velocities and pressures respectively, with P corresponding to the Lagrangian multipliers.

In such cases arbitrary combination of interpolation for pressures and velocities leads to the problem of mesh locking caused by overconstrainment, which results in rank deficiency in the coefficient matrix and a solution at best may contain spurious pressure modes or at worst be impossible to obtain. The elements with viable u and P interpolations are said to satisfy the Babuška–Brezzi (Reference 14, p. 208) condition. Two commonly used elements that satisfy this condition are shown in Figure 1. These elements are not optimal in terms of the enforcement of the incompressibility condition—or, in other words, are relatively underconstrained—which leads to poor velocity solution on coarse grids and for difficult problems.[12] Special elements with better constraint properties are discussed in Reference 12. Here the elements of Figure 1 have been chosen for the reasons of optimal convergence rate and a proven record of performance in problems of incompressible flow. These elements give C^0-continuous velocities and C^0-continuous pressures. In coupled flow and heat transfer problems a temperature degree of freedom is added with C^0-interpolation.

If we approximate (1), (4) and (3) and the boundary conditions (5)–(7) using the shape functions in (8), the final set of spatially discretized equations in a fully coupled form can be written as

$$\mathbf{M}\dot{\boldsymbol{\theta}} + \mathbf{K}\boldsymbol{\theta} = \mathbf{F}, \tag{9}$$

where $\boldsymbol{\theta}$ represents all the variables. Equation (9) may be written in an expanded matrix form as

$$\begin{bmatrix} \rho c\mathbf{M}_T & 0 & 0 & 0 \\ 0 & \rho\mathbf{M}_u & 0 & 0 \\ 0 & 0 & 0 & 0 \\ 0 & 0 & 0 & \rho\mathbf{M}_v \end{bmatrix} \begin{pmatrix} \dot{\mathbf{T}} \\ \dot{\mathbf{u}} \\ \dot{\mathbf{P}} \\ \dot{\mathbf{v}} \end{pmatrix} + \begin{bmatrix} \mathbf{K}_T & 0 & 0 & 0 \\ 0 & \mathbf{K}_{uu} & \mathbf{C}_u & \mathbf{K}_{uv} \\ 0 & \mathbf{C}_u^T & 0 & \mathbf{C}_v^T \\ \rho g\beta\mathbf{M}_v & \mathbf{K}_{vu} & \mathbf{C}_v & \mathbf{K}_{vv} \end{bmatrix} \begin{pmatrix} \mathbf{T} \\ \mathbf{u} \\ \mathbf{P} \\ \mathbf{v} \end{pmatrix} = \begin{pmatrix} \mathbf{F}_T \\ \mathbf{F}_u \\ 0 \\ \mathbf{F}_v \end{pmatrix},$$

where the first to the fourth rows represent the energy, x-momentum, continuity and y-momentum equation respectively. The matrix components are as follows.

$$\mathbf{M}_T = \mathbf{M}_u = \mathbf{M}_v = \int_\Omega N_i N_j;$$

all these matrices are $n \times n$, with n being the number of velocity and temperature interpolation nodes.

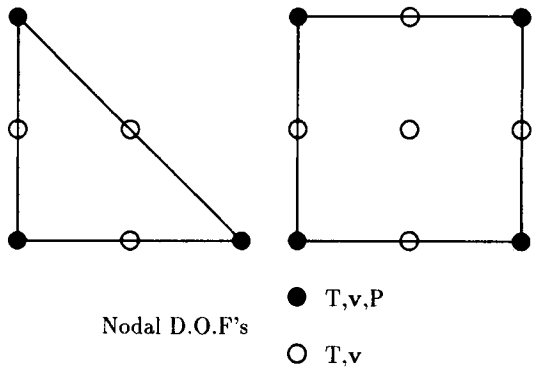

Figure 1. Elements used

$$\mathbf{K}_T=\int_\Omega \rho c\left(N_iN_ku_k\frac{\partial N_j}{\partial x}+N_iN_kv_k\frac{\partial N_j}{\partial y}\right)+k\left(\frac{\partial N_i}{\partial x}\frac{\partial N_j}{\partial x}+\frac{\partial N_i}{\partial y}\frac{\partial N_j}{\partial y}\right)+\int_\Gamma h(N_iN_j),$$

$$\mathbf{K}_{uu}=\int_\Omega \rho\left(N_iN_ku_k\frac{\partial N_j}{\partial x}+N_iN_kv_k\frac{\partial N_j}{\partial y}\right)+\mu\left(2\frac{\partial N_i}{\partial x}\frac{\partial N_j}{\partial x}+\frac{\partial N_i}{\partial y}\frac{\partial N_j}{\partial y}\right),$$

$$\mathbf{K}_{vv}=\int_\Omega \rho\left(N_iN_ku_k\frac{\partial N_j}{\partial x}+N_iN_kv_k\frac{\partial N_j}{\partial y}\right)+\mu\left(\frac{\partial N_i}{\partial x}\frac{\partial N_j}{\partial x}+2\frac{\partial N_i}{\partial y}\frac{\partial N_j}{\partial y}\right),$$

$$\mathbf{K}_{uv}=\int_\Omega \mu\left(\frac{\partial N_i}{\partial y}\frac{\partial N_j}{\partial x}\right),\qquad \mathbf{K}_{vu}=\int_\Omega \mu\left(\frac{\partial N_i}{\partial x}\frac{\partial N_j}{\partial y}\right);$$

all the above are $n\times n$ matrices.

$$\mathbf{C}_u=-\int_\Omega \frac{\partial N_i}{\partial x}N_j',\qquad \mathbf{C}_v=-\int_\Omega \frac{\partial N_i}{\partial y}N_j';$$

these are $n\times n'$ matrices.

$$\mathbf{C}_u^T=\int_\Omega N_i'\frac{\partial N_j}{\partial x},\qquad \mathbf{C}_v^T=\int_\Omega N_i'\frac{\partial N_j}{\partial y};$$

these are $n'\times n$ matrices. Finally, the force vectors, which are all n-vectors, are

$$\mathbf{F}_T=\int_\Omega N_i\dot{Q}-\int_\Gamma N_i(q-hT_a),\qquad \mathbf{F}_u=\int_\Gamma N_if_x,\qquad \mathbf{F}_v=\int_\Gamma N_if_y+\rho g\beta\mathbf{M}_vT_r.$$

This completes the spatial discretization by the finite element method of the original conservation equations in a standard manner.

4.2. Temporal discretization

The spatial discretization discussed in the previous subsection creates a set of first-order ordinary differential equations with respect to time. The first-order system of equations represented by (9) can be discretized in time by the 'generalized midpoint or trapezoidal family of methods' (Reference 16, p. 145):

$$\mathbf{M}(\boldsymbol{\theta}_{n+\alpha},t_{n+\alpha})\dot{\boldsymbol{\theta}}_{n+\alpha}+\mathbf{K}(\boldsymbol{\theta}_{n+\alpha},t_{n+\alpha})\boldsymbol{\theta}_{n+\alpha}=\mathbf{F}(\boldsymbol{\theta}_{n+\alpha},t_{n+\alpha}),\tag{10}$$

where n is the time step number and

$$\boldsymbol{\theta}_{n+\alpha}=(1-\alpha)\boldsymbol{\theta}_n+\alpha\boldsymbol{\theta}_{n+1},\qquad \dot{\boldsymbol{\theta}}_{n+\alpha}=\frac{\boldsymbol{\theta}_{n+1}-\boldsymbol{\theta}_n}{\Delta t},\qquad t_{n+\alpha}=t_n+\alpha\Delta t.\tag{11}$$

Substituting (11) into (10), we obtain

$$(\mathbf{M}_{n+\alpha}+\alpha\Delta t\mathbf{K}_{n+\alpha})\boldsymbol{\theta}_{n+1}=[\mathbf{M}_{n+\alpha}-(1-\alpha)\Delta t\mathbf{K}_{n+\alpha}]\boldsymbol{\theta}_n+\Delta t\mathbf{F}_{n+\alpha}.\tag{12}$$

By changing the value of α from zero to unity, different members of this family of methods are identified, i.e.

$\alpha=0$,	forward difference or forward Euler
$\alpha=\frac{1}{2}$,	midpoint rule or Crank–Nicolson
$\alpha=\frac{2}{3}$,	Galerkin
$\alpha=1$,	backward difference or backward Euler.

All except the first (forward Euler) of the above schemes are implicit, i.e. they require matrix inversion for solution.

Rigorous analysis of the stability and convergence characteristics of non-linear convection/diffusion problems which involve non-symmetric and non-positive definite matrices is not a simple matter. Useful information can be found in the relevant literature such as Reference 16. Some results obtained from an energy method analysis (Reference 16, p. 150) suggest unconditional stability for $\alpha \geqslant \frac{1}{2}$ for the generalized midpoint family.

5. MODELLING OF THE LATENT HEAT EFFECT

Among the fixed mesh methods, the most commonly used methods have been 'effective heat capacity' and the 'enthalpy method'. In the first method a temperature-dependent specific heat over a range of temperatures is used to account for the extra heat generated/absorbed due to phase change. This method therefore cannot accurately model an isothermal change of phase owing to the requirement of a temperature range. In reality this method is of limited value in cases other than those where the phase change occurs in a very wide range of temperatures, owing to limitations on temporal and spatial step sizes, problems of convergence and oscillation, etc.[17] The enthalpy method[2] enables the heat capacity to be defined as a smooth function of temperature,

$$\rho c = \frac{\mathrm{d}H}{\mathrm{d}T}, \tag{13}$$

where H represents enthalpy. This is calculated using several averaging techniques.[17] The technique suggested in Reference 2 is simple and gives satisfactory results, i.e.

$$(\rho c)_n = \frac{H_n - H_{n-1}}{T_n - T_{n-1}}, \tag{14}$$

where n represents the time step number. The enthalpy method also suffers from the limitation that the phase change must occur over a temperature range.

A more suitable method is the 'fictitious heat flow method'[10] whereby all the latent heat available at the nodes is lumped and released as an internal heat source at the appropriate temperature or in a range of temperatures, which enables the modelling of isothermal phase changes as well as those over a range of temperatures. To implement this method in the numerical scheme, the $\dot{Q}$-term (which is the rate of internal heat generation) from the energy equation (3) is used by specifying

$$\dot{Q} = \rho \dot{L},$$

where L is the latent heat. The total latent heat available at each node i of the finite element mesh, say Q_{tot_i} is calculated according to the volume V_i associated with the node i, which can be obtained by constructing a lumped mass matrix.[13] At a given time step Δt_n the $\dot{Q}_i$-term for node i in the force vector is calculated for each iteration p as

$$\dot{Q}_i^p = \frac{\rho c}{\Delta t_n} V_i (T_{\mathrm{f}} - T_i),$$

where T_{f} is the freezing temperature for an isothermal phase change; for a mushy phase change it can be either the liquidus temperature in the case of freezing or the solidus temperature in the case of melting. The above equation is only used if the temperature after any iteration enters the phase change range. The total latent heat accounted over the time step Δt_n is the sum of $\dot{Q}_i^p$ for all

iterations times Δt_n. This enables the use of variable time steps in the analysis. The phase change is considered complete after all the latent heat is accounted for over one or more time steps. This method gives very reasonable results even for large time steps and coarse meshes.

Figure 2 shows comparisons between the analytical solution of the enthalpy and the source methods for a 1D solidification problem as in Reference 10. The material properties are shown in the figure; T_0 and T_f refer to the initial and freezing temperatures respectively. Although the enthalpy method appears to be relatively more accurate, the source method gave reasonable results in less than 5% of the time. Furthermore, a 1 °C temperature range was used for the enthalpy method while for the source method the phase change was isothermal. A more accurate solution may be obtained using the source method if smaller time steps are used.

6. VELOCITY SUPPRESSION IN THE SOLIDIFIED REGION

Since the Navier–Stokes equation is being solved for the whole domain, there needs to be a mechanism for suppressing the velocities in the areas which are solid. The simplest method[7] is to assign the nodal velocity values to zero where the nodal temperature is below the freezing or solidus temperature (T_s). A more rigorous approach is used in Reference 9, which consists of modelling the mushy zone as a porous medium and making the porosity (ε) depend on the amount of latent heat released/absorbed. The flow in the porous medium (mushy zone) is then governed by the momentum equations and a source term obtained from Darcy's law. A less sophisticated and easier-to-implement approach was used in Reference 6, which involves making the viscosity a function of temperature, so that when the temperature goes from the liquidus (T_l) to the solidus the viscosity increases rapidly to a 'large' value. This causes the velocities in the

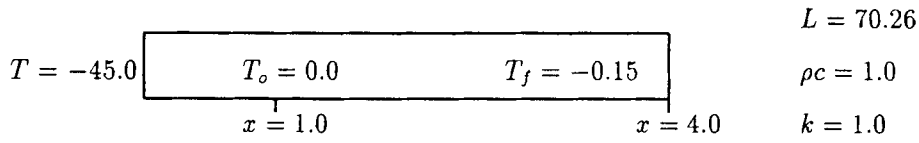

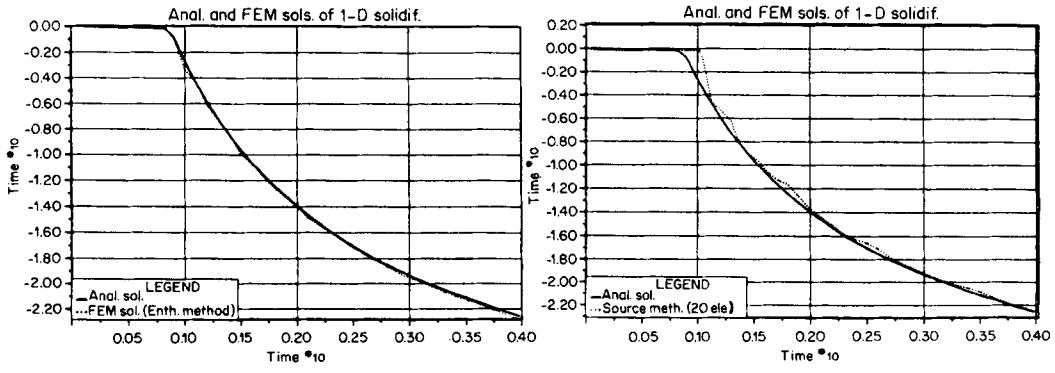

From 1500 Timesteps From 70 Timesteps

Figure 2. Comparison of the enthalpy and source methods (temperature versus time at $x = 1{\cdot}0$)

corresponding areas to be suppressed. Following the last approach, in this work the mushy zone viscosity μ_m is made a function of temperature as

$$\mu_m = \mu_l \left(\frac{\mu_s}{\mu_l} \right)^{(T_l - T)/(T_l - T_s)},$$

where μ_s is the viscosity in the solid region (fixed to a large number) and μ_l is the viscosity in the liquid region.

7. NUMERICAL EXAMPLES

Some examples of solidification and melting in a cavity are solved using a finite element programme developed according to the preceding theory. Firstly, properties roughly those of an aluminium alloy have been used, with the phase change assumed to happen over a 25 °C range. Three examples have been solved, which include solidification of the above alloy in the cavity with natural convection effects, followed by melting in the same cavity and finally simultaneous solidification and melting.

Secondly, isothermal solidification of water in a square cavity has been analysed taking into account the density extremum of water at 4·0 °C. The results have been compared with those of Davis *et al.*[18]

All the examples were solved using both lumped and consistent capacitance matrices. Only the lumped mass results have been presented since they were smoother; there was little difference in the two solutions otherwise. The backward Euler method ($\alpha = 1$) was used for time integration in all examples. The finite element mesh used for all problems is shown in Figure 3.

7.1. Solidification example

We begin with an example of the solidification of an aluminium alloy in a square cavity (5·0 cm × 5·0 cm) as shown in Figure 4. The material properties and the boundary conditions are

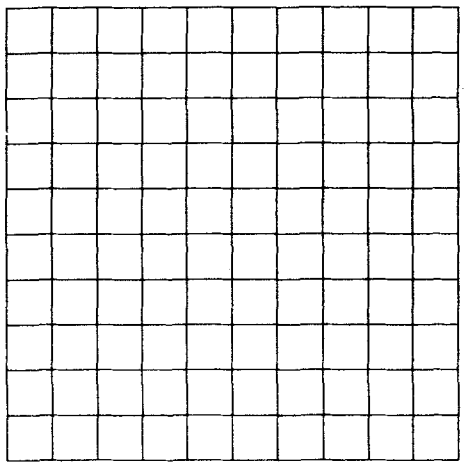

Figure 3. Finite element mesh for the problems of solidification and melting of aluminium and isothermal solidification of water

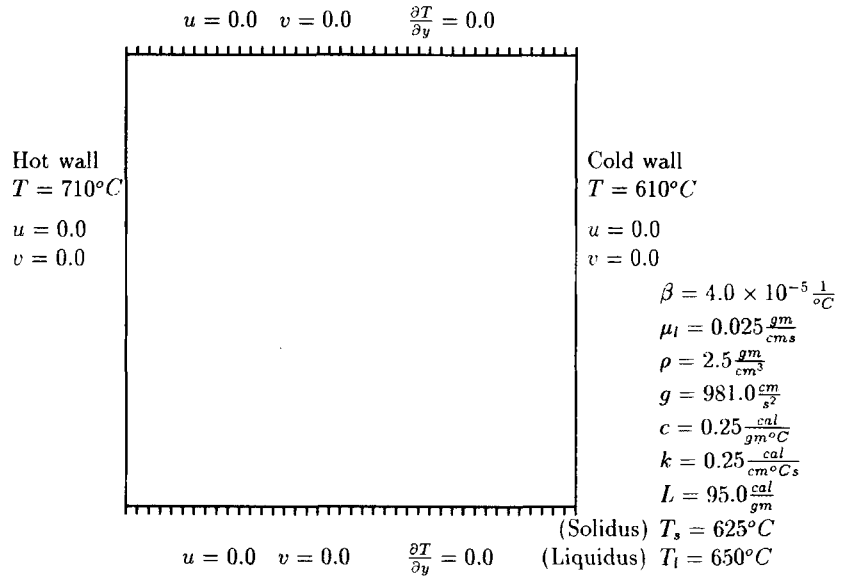

Figure 4. The problem domain with boundary conditions and material properties for aluminium alloy

also shown in the figure. The phase change is assumed to occur over a range of 25 °C. The material properties, boundary conditions and cavity dimensions correspond to a Rayleigh number (*Ra*) of $1{\cdot}2 \times 10^5$, a Prandtl number (*Pr*) of 0·02 and a Stefan number (*Ste*) of 0·22. The Stefan number (*Ste*) is a measure of the amount of sensible heat compared to latent heat, i.e.

$$Ste = \frac{c\Delta T}{L},$$

where ΔT is the absolute difference between the cold wall and phase change temperatures in the case of solidification and between the hot wall and phase change temperatures in the case of melting. The lower *Ste* is, the more difficult the phase change problem becomes. We begin with liquid at a uniform initial temperature over the whole domain which is equal to the hot wall temperature (710 °C). The same thermal properties have been used for the liquid and solid and, to further simplify matters, have been assumed constant. The solid viscosity was fixed arbitrarily at 10^5, which was sufficient to suppress flow in the solid regions.

The results of several time steps from this analysis are shown in Figure 5 in the form of velocity vectors and temperature contours. The last set of results represents a steady state after which the solution remains essentially uniform.

7.2. Melting example

The same alloy as used in the previous subsection is now melted. The boundary conditions are kept the same as before. Here we begin with a uniform initial temperature equal to the cold wall temperature (610 °C), which is below the solidus temperature (625 °C), thus making the whole domain solid.

The results of several time steps from this analysis are shown in Figure 6. Again the last set of results represents a steady state. It may be noted that the steady state result from the last example

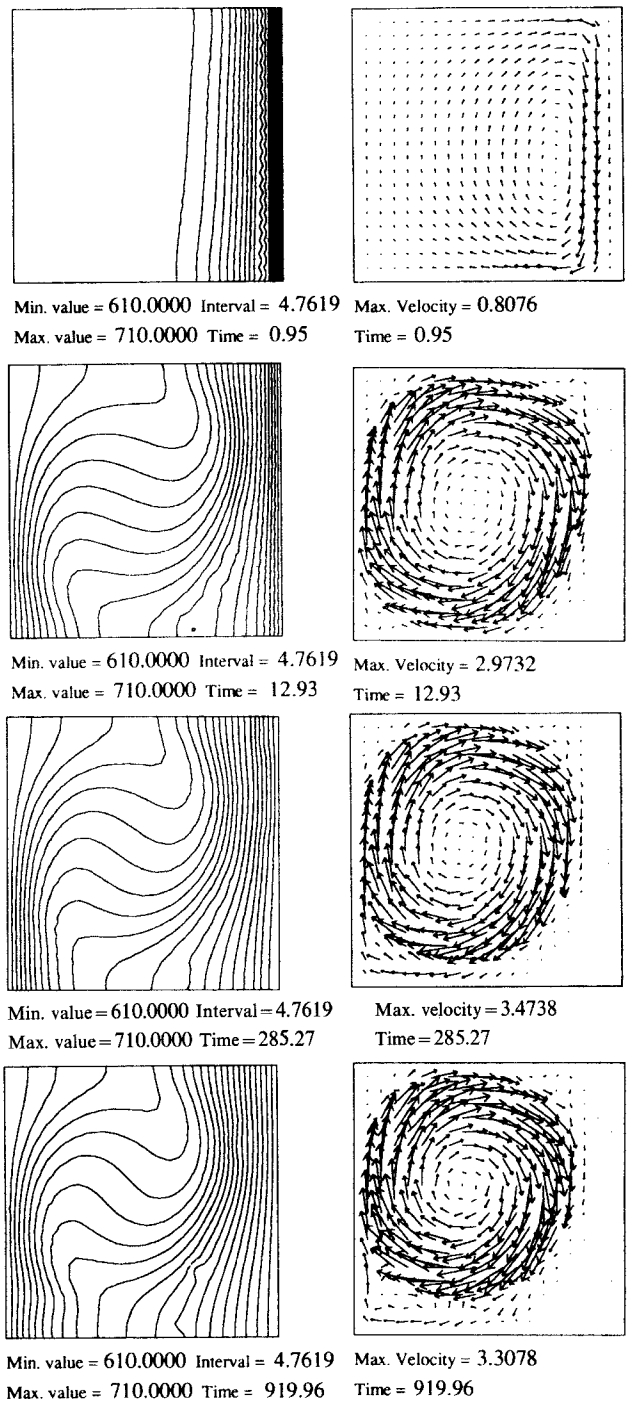

Figure 5. Results from the solidification example

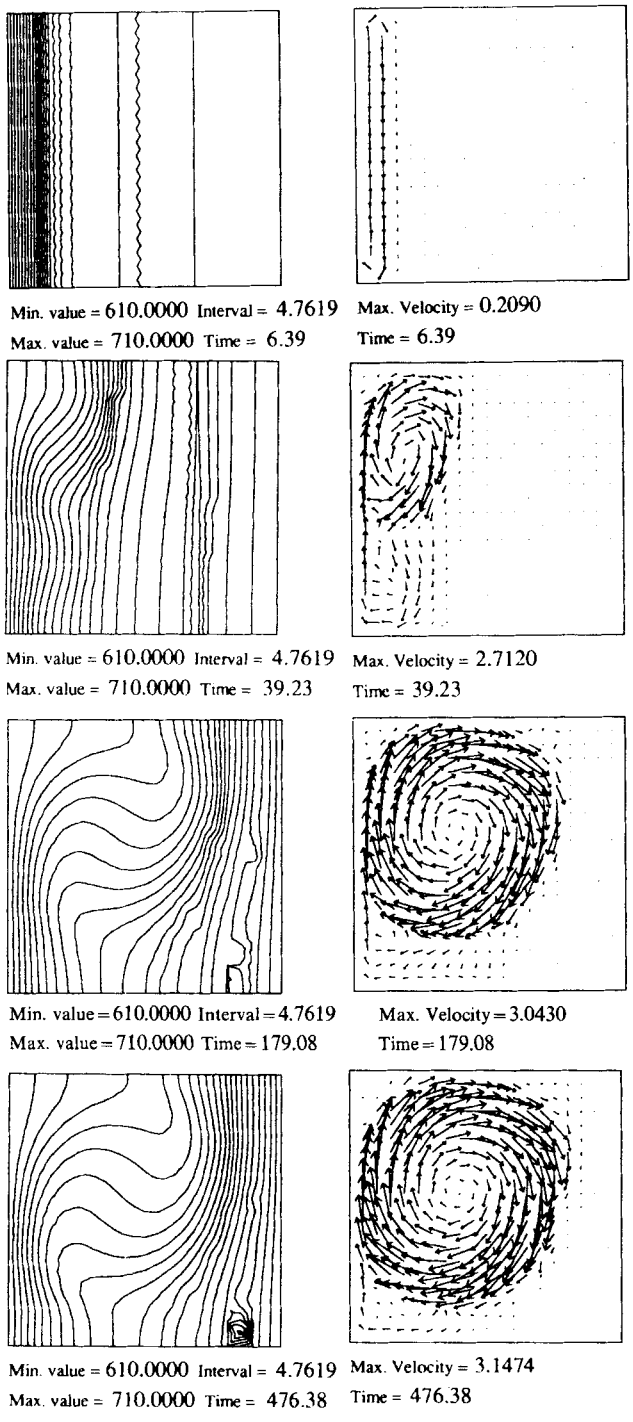

Figure 6. Results from the melting example

is quite similar to this one, which of course must be the case since the boundary conditions are the same.

There is evidence of wiggles in some of the isotherm plots, mainly because of two reasons. Firstly, in the areas undergoing phase change the temperature correction involved in the heat source algorithm produces some local wiggles in the contours. Secondly, the use of lumped mass matrices also causes wiggles (oscillations) in transient advection problems.[19] The unphysical isolated peak in the solidified region of the last isotherm plot of Figure 6 is due to the first, as it lies within the phase change region.

7.3. Combined solidification and melting example

The same alloy with the same boundary conditions is now analysed with an initial condition as shown in Figure 7, where the domain is partly solid and partly liquid, with the solid part at an initial temperature equal to the cold wall temperature (610 °C) and the liquid part at an initial temperature equal to the hot wall temperature (710 °C). This means that the steady state solution can only be reached if solidification and melting occur simultaneously.

Figure 8 shows the results of a few time steps from this analysis. It may be noted that the bottom half of the liquid region freezes initially owing to the loss of heat to the solid region, but melts again later with the build-up of heat as the parts of the solid region begin to melt as well. It can again be seen that the steady state result here corresponds to the previous ones from Figures 5 and 6. Again the wiggles seen in the isotherm plots of Figure 8 can be explained by the reasoning given in the previous subsection.

7.4. Isothermal solidification of water accounting for the density anomaly

A more challenging example is now solved to assess the capabilities of the programme. This example involves the solidification of water in the square cavity. Phase change takes place

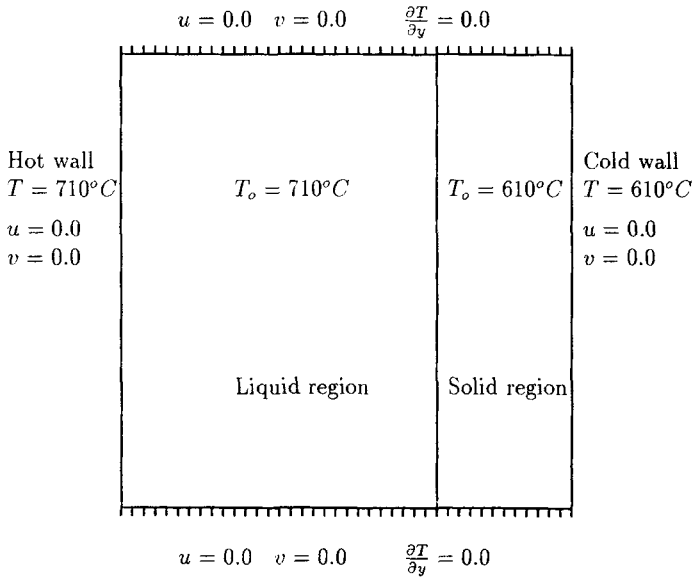

Figure 7. Problem domain for the combined solidification and melting example

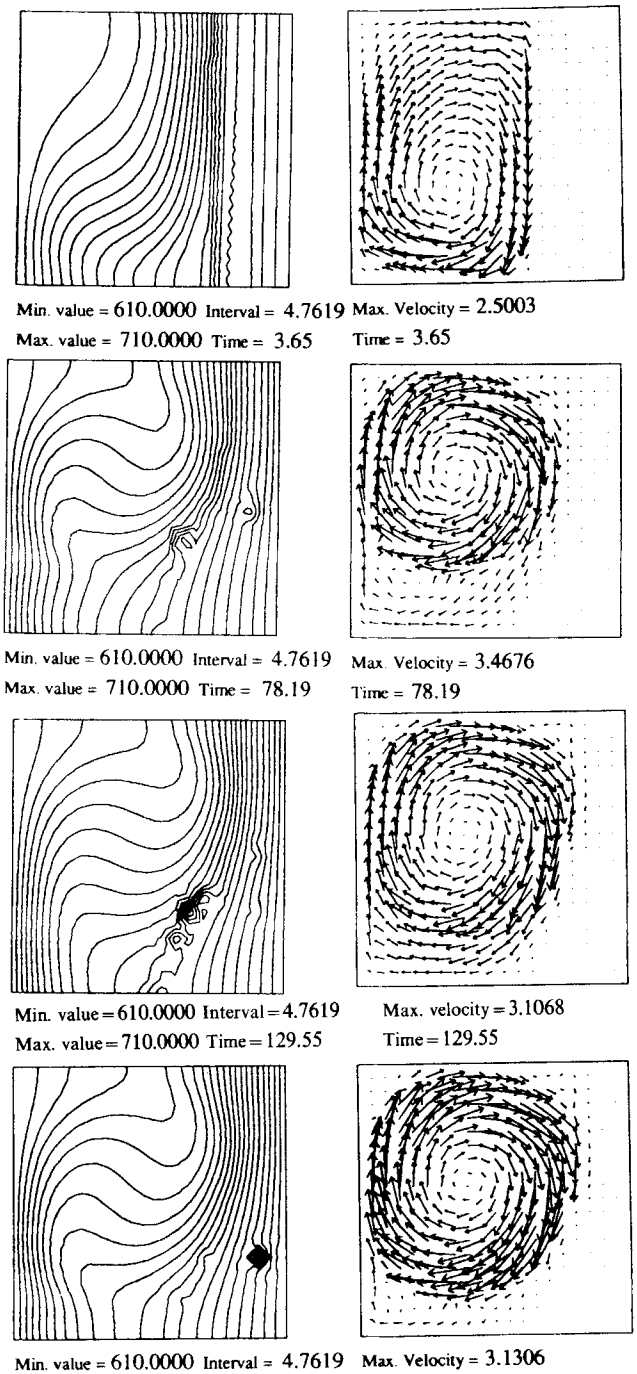

Figure 8. Results from the combined solidification and melting example

isothermally at 0 °C, which poses no problem since the source method is used. This analysis is complicated by the anomalous behaviour of water between the temperatures of 4 and 0 °C, when it expands upon cooling. Therefore the density of water decreases below 4 °C and reverse buoyancy forces are generated. In accordance with the Boussinesq approximation we deal with this problem by keeping the density constant and varying the thermal coefficient β. This is done by using the equation of state which relates density and temperature as

$$\rho(T)=\rho_0[1-\beta(T-T_r)],$$

where ρ_0 is the density at which the buoyancy forces are zero, corresponding to a temperature T_r. Differentiating this equation with respect to temperature and rearranging, we obtain

$$\beta(T)=-\frac{1}{\rho_0}\frac{\mathrm{d}\rho}{\mathrm{d}T}. \tag{15}$$

This equation can be used with the following relation from Reference 20 to obtain β in terms of temperature:

$$\rho(T)=0{\cdot}999\,878\,383+(5{\cdot}353\,697T-0{\cdot}690\,752T^2+0{\cdot}003\,641T^3)\times 10^{-5},$$

from which we can write

$$\frac{\mathrm{d}\rho}{\mathrm{d}T}=(5{\cdot}353\,697-1{\cdot}381\,504T+0{\cdot}010\,923T^2)\times 10^{-5}.$$

In addition to the buoyancy variation as described above, the temperature-dependent viscosity according to another relation from Reference 20 has been used, i.e.

$$\mu(T)=\mu_r\exp\left[6{\cdot}18\times 10^7\left(\frac{1}{T^3}-\frac{1}{T_r^3}\right)\right],$$

where μ_r is a reference viscosity corresponding to a temperature T_r.

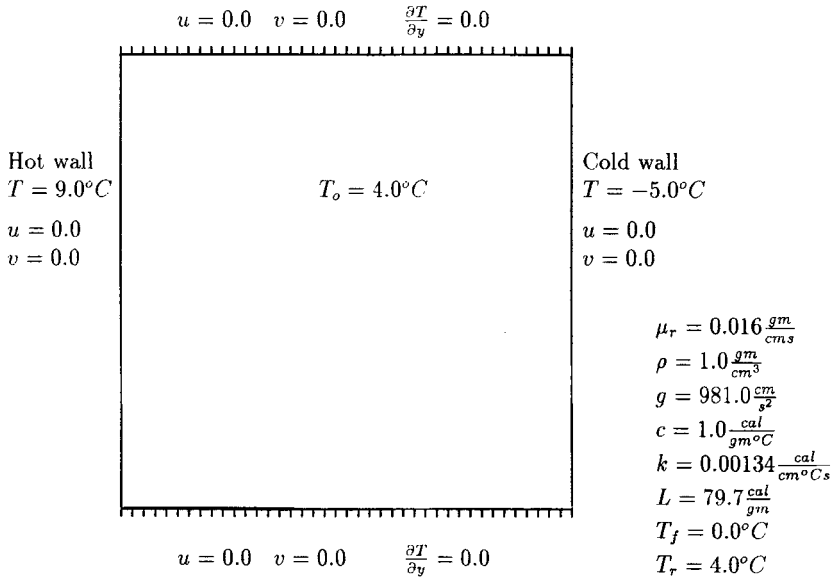

Figure 9. The problem domain for isothermal freezing of water

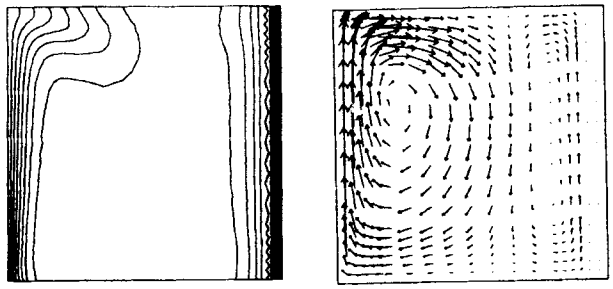

Min. value = -5.0000 Interval = 0.6667
Max. value = 9.0000 Time = 29.78

Max. Velocity = 0.0950
Time = 29.78

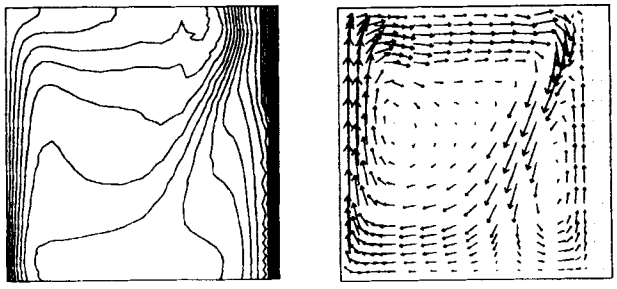

Min. value = -5.0000 Interval = 0.6667
Max. value = 9.0000 Time = 184.19

Max. Velocity = 0.0840
Time = 184.19

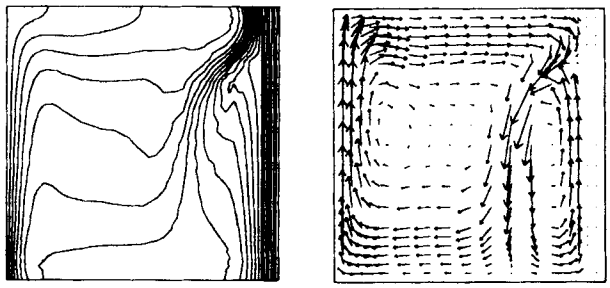

Min. value = -5.0000 Interval = 0.6667
Max. value = 9.0000 Time = 247 05

Max. Velocity = 0.0814
Time = 247.05

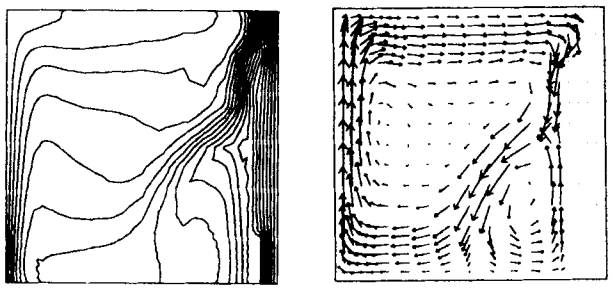

Min. value = -5.0000 Interval = 0.6667
Max. value = 9.0000 Time = 654.77

Max. Velocity = 0.0754
Time = 654.77

Figure 10. Results from isothermal solidification of water

Figure 9 shows the problem domain, which again is a square cavity of size 3·0 cm × 3·0 cm, and the boundary conditions and material properties. *Ra* is about 10^6, the *Pr* is about 12·0 and *Ste* is about 0·11. Figure 10 shows the results of a few time steps from this analysis. These results appear to be in agreement with the numerical results of Davis *et al.*,[18] who have presented their results in the form of streamlines and temperature contours for three different times, which are reproduced in Figure 11. Davis *et al.* have compared their results with a flow visualization result of Weaver and Viskanta,[21] which is shown in Figure 12.

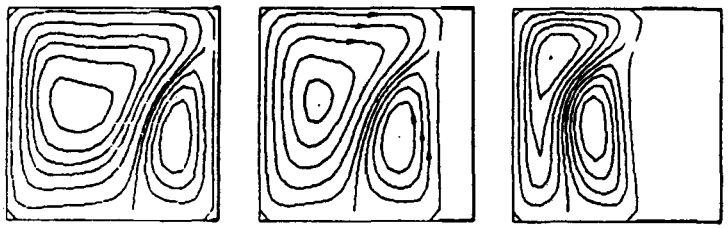

(a) (b) (c)

Streamlines during the freezing of water: (a) $t = 0$ (b) $t = 4.25$min. (c) $t = 34$ min.

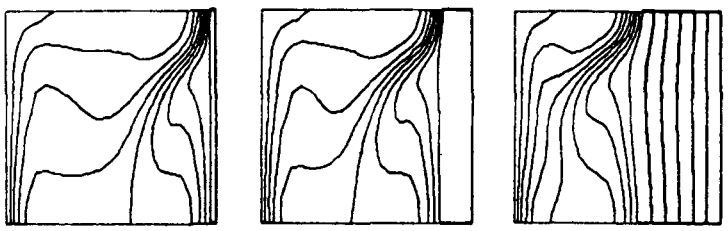

(a) (b) (c)

Isotherms during the freezing of water: (a) $t = 0$ (b) $t = 4.25$min. (c) $t = 34$ min.

Figure 11. Numerical results of Davis *et al.*[18] for isothermal solidification of water

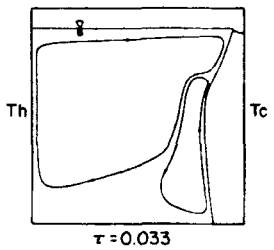

Figure 12. Flow visualization result of Weaver and Viskanta[21] for solidification of water

8. CONCLUSIONS

It is evident from the problems solved in the previous section that a fixed-grid-based finite element method as presented earlier combined with the source method for latent heat release/absorption is capable of providing good quality analyses of a wide variety of problems of phase change in the presence of natural convection.

These problems were solved using both lumped and consistent mass matrices. As reported in Reference 10, the lumped mass matrices gave a smoother solution. Although lumped mass matrices cause oscillations in the case of transient advection,[19] it appears that their smoothing effect in latent heat evolution outweighs the deleterious effect in advection. The unphysical local peaks that appeared in the solidified regions in some of the isotherm plots are probably due to the mesh, which is quite coarse. Some wiggles were generated as a result of the temperature correction that is required in the heat-source-based latent heat algorithm at the end of each iteration. This effect can be reduced if a finer mesh is used in the phase change region,[22] since the heat source method produces smoother results with finer meshes. A finer mesh than the one used here would also produce smoother velocity plots.

REFERENCES

1. R. W. Lewis and P. M. Roberts, 'Finite element simulation of solidification problems', *Appl. Sci. Res.*, **44**, 61–92 (1987).
2. K. Morgan, R. W. Lewis and O. C. Zienkiewicz, 'An improved algorithm for heat conduction problems with phase change', *Int. j. numer. methods eng.*, **12**, 1191–1195 (1978).
3. R. Viskanta, 'Natural convection in melting and solidification', in S. Kakac, W. Aung and R. Viskanta (eds), *Natural Convection: Fundamentals and Applications*, Hemisphere, Washington, DC, 1985, pp. 845–877.
4. E. M. Sparrow, S. V. Patankar and S. Ramadhyani, 'Analysis of melting in the presence of natural convection in the melt region', *ASME J. Heat Transfer*, **99**, 520–526 (1977).
5. E. M. Sparrow, J. M. Ramsey and R. G. Kemink, 'Freezing controlled by natural convection', *ASME J. Heat Transfer*, **101**, 578–584 (1979).
6. D. K. Gartling, 'Finite element analysis of convective heat transfer problems with change of phase', in K. Morgan, C. Taylor and C. A. Brebbia (eds), *Computer Methods in Fluids*, Pentech, London, 1980, pp. 489–500.
7. K. Morgan, 'A numerical analysis of freezing and melting with convection', *Comput. Methods Appl. Mech. Eng.*, **28**, 275–284 (1981).
8. R. Viskanta, 'Phase change heat transfer', in G. A. Lane (ed.), *Solar Heat Storage Latent Heat Materials*, CRC Press, Boca Raton, FL, 1983, pp. 153–222.
9. V. R. Voller, M. Cross and N. C. Markatos, 'An enthalpy method for convection/diffusion phase change', *Int. j. numer. methods eng.*, **24**, 271–284 (1987).
10. W. D. Rolph and K. J. Bathe, 'An efficient algorithm for analysis of nonlinear heat transfer with phase changes', *Int. j. numer. methods eng.*, **18**, 119–134 (1982).
11. P. M. Gresho, R. L. Lee, S. T. Chan and R. L. Sani, 'Solution of the time-dependent Navier–Stokes and Boussinesq equations using the Galerkin finite element method', *Proc. IUTAM Symp. on Approximation Methods for Navier–Stokes Problems*, Paderborn, September 1979, Springer, pp. 203–222.
12. P. M. Gresho, R. L. Lee and R. L. Sani, 'On the time-dependent solution of the incompressible Navier–Stokes equations in two and three dimensions', in *Recent Advances in Numerical Methods in Fluids, Vol. 1*, Pineridge, Swansea, 1980, pp. 27–79.
13. O. C. Zienkiewicz, *The Finite Element Method*, McGraw-Hill, London, 1977.
14. T. J. R. Hughes, *The Finite Element Method—Linear Static and Dynamic Finite Element Analysis*, Prentice-Hall, Englewood Cliffs, NJ, 1987.
15. O. C. Zienkiewicz, R. L. Taylor and J. A. W. Baynham, 'Mixed and irreducible formulations in finite element analysis', in S. N. Atluri, R. H. Gallagher and O. C. Zienkiewicz (eds), *Hybrid and Mixed Finite Element Methods*, Wiley, 1983.
16. T. J. R. Hughes, 'Analysis of transient algorithms with particular reference to stability behaviour', in *Computational Methods for Transient Analysis*, Elsevier, 1983.
17. A. J. Dalhuijsen and A. Segal, 'Comparison of finite element techniques for solidification problems', *Int. j. numer. methods eng.*, **23**, 1807–1829 (1986).
18. G. V. Davis, E. Leonardi, P. H. Wong and G. H. Yeoh, 'Natural convection in a solidifying liquid', *Sixth Int. Conf. for Numerical Methods in Thermal Problems*, Swansea, July 1989, Pineridge, Swansea, pp. 410–420.
19. P. Gresho and R. L. Lee, 'Don't suppress the wiggles—they are telling you something!', *Comput. Fluids*, **9**, 223–253 (1981).

20. J. A. Reizes, E. Leonardi and G. V. Davis, 'Natural convection near the density extremum of water', *Numerical Methods in Laminar and Turbulent Flow*, Swansea, July 1985, Pineridge, Swansea.
21. J. A. Weaver and R. Viskanta, 'Freezing of water saturated porous media in a rectangular cavity', *Int. Commun. Heat Mass Transfer*, **13**, 245–521 (1986).
22. R. W. Lewis, H. C. Huang and A. S. Usmani, 'Remeshing approaches to finite element simulation of casting problems', *Eurotherm Seminar No. 6, Heat Transfer in Phase Change Problems*, Delft, October, TUDelft, 1988, pp. 37–39.